RESEARCH ARTICLE
PLANETARY SCIENCES

Earth and Planetary Physics
7: 421–435, 2023
doi: 10.26464/epp2023045

Spacecraft potential variations of the Swarm satellites at low Earth orbital altitudes

HaiCheng Jiang[1], Chao Xiong[1,2*], Fan Yin[1], YuHao Zheng[1], ZiYuan Zhu[1], Rui Yan[3], and YiWen Liu[4]

[1]Department of Space Physics, Electronic Information School, Wuhan University, Wuhan 430072, China;

[2]Hubei Luojia Laboratory, Wuhan 430079, China;

[3]National Institute of Natural Hazards, the Ministry of Emergency Management of China, Beijing 100085, China;

[4]School of Physics and Electronic Information, Shangrao Normal University, Shangrao 334001, China

Key Points:

- We provide the first detailed analysis of variations in the spacecraft potential (V_s) of Swarm satellites, showing V_s falling within a few negative volts.
- The Swarm V_s data show two peaks centered around −2 V and −5.5 V, and the two V_s categories exhibit different spatial and temporal distributions.
- We suggest the two V_s categories are dominated by the background "cold" plasma (due to ionization) and "hot" plasma (due to precipitated particles from magnetosphere), respectively.

Citation: Jiang, H. C., Xiong, C., Yin, F., Zheng, Y. H., Zhu, Z. Y., Yan, R., and Liu, Y. W. (2023). Spacecraft potential variations of the Swarm satellites at low Earth orbital altitudes. *Earth Planet. Phys.*, *7*(4), 421–435. http://doi.org/10.26464/epp2023045

Abstract: In this study, we provide the first detailed analysis of variations in the spacecraft potential (V_s) of the three Swarm satellites, which are flying at about 400–500 km. Unlike previous studies that have investigated extreme charging events, usually with spacecraft potentials as negative as −100 V, this study is focused on variations of Swarm V_s readings, which fall within a few negative volts. The Swarm observations show that spacecraft at low Earth orbital (LEO) altitudes are charged only slightly negatively, varying between −7 V and 0 V, with the majority of recorded potentials at these altitudes clustering close to −2 V. However, a second peak of V_s data is found at −5.5 V, though the event numbers for these more-negative observations are less, by an order of magnitude, than for incidents near the −2 V peak. These two distinct V_s peaks suggest two different causes. We have thus divided the Swarm spacecraft V_s data into two categories: less-negatively charged ($-5 < V_s < 0$ V) and more-negatively-charged ($-6.5 < V_s < -5$ V). These two V_s categories exhibit different spatial and temporal distributions. The V_s observations in the first category remain relatively closer to 0 V above the magnetic equator, but become much more negative at low and middle latitudes on the day side; at high latitudes, these first-category V_s readings are relatively more-negative during local summer. Second-category V_s events cluster into two bands at the middle latitudes (between ±20°–50° magnetic latitude), but with slightly more negative readings at the South Atlantic Anomaly (SAA) region; at high latitudes, these rarer but more-negative second-category V_s events exhibit relatively more-negative values during local winter, which is opposite to the seasonal pattern seen in the first category. By comparing V_s data to the distributions of background plasma density at Swarm altitudes, we find for the first category that more-negative V_s readings are recorded at regions with higher background plasma density, while for the second category the more-negative V_s data are observed at regions with lower background plasma density. This can be explained as follows: the electron and ion fluxes incident on Swarm surface, whose differences determine the potential of Swarm, are dominated by the background "cold" plasma (due to ionization) and "hot" plasma (due to precipitated particles from magnetosphere) for the two V_s categories, respectively.

Keywords: spacecraft potentia; low Earth orbit satellites; Swarm mission; particle precipitation

1. Introduction

When flying in space, a spacecraft interacts with the ambient plasma. The electrons, with relatively lighter mass, are usually much more mobile than the ions; therefore, the ambient electron flux received by a spacecraft exceeds the ambient ion flux by typically two orders of magnitude, resulting in a slightly negatively charged spacecraft surface (Garrett, 1981). In some specific regions, the electrons can be accelerated to a very high energy level, causing the spacecraft potential to reach as low as −1000 V (Frooninckx and Sojka, 1992). Due to different geometry and dielectric properties of the surface material, as well as different light conditions from different directions, charging can also occur between panels of the spacecraft surface, or between the surface

First author: H. C. Jiang, hc_jiang@whu.edu.cn
Correspondence to: C. Xiong, xiongchao@whu.edu.cn
Received 27 DEC 2022; Accepted 17 APR 2023.
Accepted article online 13 JUN 2023.

and the spacecraft's ground potential, resulting in potential differences between different spacecraft panels. When the potential difference reaches a certain threshold, electrostatic discharge will be generated. Such charging and discharging processes may directly, or indirectly through electromagnetic radiation, affect the onboard electronic equipment, or even cause circuit failure, threatening the safety of the entire spacecraft (Lai ST and Cahoy, 2016).

Spacecraft charging can be generally classified into two types: surface charging and deep dielectric charging (Garrett, 1981). "Deep dielectric charging" refers to bulk charging or internal charging. To produce deep dielectric charging, a large amount of electron energy is required, sufficient to penetrate the spacecraft's surface material and reach inside the spacecraft. Less than 100 keV of electron energy is required for surface charging; to cause deep dielectric charging requires greater than 500 keV (Anderson, 2012). More energetic particles are distributed in the Earth's magnetosphere, especially in the radiation belt (Ye YG et al., 2021); thus, significant spacecraft charging has often been observed in satellites flying at high and medium orbits. For example, the Geosynchronous Earth Orbit (GEO) ATS 5 was found, during an eclipse, to be charged to more than 10,000 V (DeForest, 1972). Another example of a spacecraft failure due to charging is the Galaxy 15, which was launched in 2005 with an expected operational lifetime of 15 years. On 5th April 2010, during a geomagnetic storm, the satellite ceased responding to ground commands. It was suggested that the failure was caused not only by the generally high level of geomagnetic activity (minimum *Dst* reaching −81 nT), but also, and perhaps more critically, because the position of the Galaxy 15, at the time of failure, subjected it to the particularly high energy electron injections recorded at the polar region (Allen, 2010).

A dedicated mission, e.g., the Spacecraft Charging AT High Altitudes (SCATHA), was launched to predict and/or model the charging effects on synchronous and near synchronous satellites. It provided years of data that are still being analyzed today, greatly expanding our understanding of how charging occuring on a spacecraft's surface. Analysis shows that high spacecraft frame potentials are correlated with 10 to 50 keV electron fluxes, especially when these fluxes exceed 1×10^8 cm^{-2} s^{-1} sr^{-1}. Four criteria have been used to select severe environments at high Earth orbit altitudes: (1) large fluxes of electrons with energies above 10 keV; (2) large fluxes of electrons with energies below 50 keV and above 200 keV; (3) large fluxes of electrons with energies below 50 keV and low fluxes with energies above 200 keV; and (4) long periods of time with a spacecraft potential below −5 kV (Matéo-Vélez et al., 2018).

At low Earth orbit (LEO) satellite altitudes, the electron and ion energies are much lower; therefore, surface charging of LEO satellites has been thought to be not as severe as that at the high and middle Earth orbits. However, Anderson (2012) reported that Defense Meteorological Satellite Program (DMSP) spacecraft flying at 840 km can sometimes charge to very large negative voltages (as low as −2000 V) when encountering intense precipitating electrons, e.g., inside the auroral arcs. By analyzing data from an 11-year period DMSP satellite observations, Anderson (2012) found over 1600 charging events, defined as spacecraft charged more negative than −100 V during the auroral crossing. These charging events observed by DMSP satellites happened mainly at auroral latitudes from dusk to pre-midnight hours, and during low solar activity years when the background plasma density was lower than 10^{10} m^{-3}. Charging events have also been observed on the International Space Station (Wright et al., 2008). These findings revealed that energetic particles can threaten LEO satellites, especially when LEO satellites enter the auroral region, or during intense geomagnetic storms.

In this study, we performed an analysis of spacecraft potential variations recorded by the European Space Agency (ESA)'s Swarm satellites flying at 400–500 km altitudes. Rather than focusing on the very negative charging events observed in the auroral region, we surveyed in detail the potential variations observed by Swarm spacecraft over all latitudes. We find that, although the spacecraft potential of Swarm satellites varies mainly within a few negative volts, the data exhibit distinct spatiotemporal distribution characteristics. In addition, the Swarm constellation with three satellites flying at different altitudes can also provide a direct comparison of the space environment influence on the potentials of LEO satellites at different altitudes. This paper follows the traditional structure. First, we introduce the data we analyzed and the instruments used to collect these data. Subsequently, we present our observations and discuss the results. Finally, we summarize our main findings and conclusions.

2. Dataset and Processing Approaches

2.1 Swarm Satellite and Electric Field Instruments (EFI) Package

ESA's Swarm mission, consisting of three identical satellites, was launched into a near-polar circular orbit on 22 November 2013. From January 2014 onward the three spacecraft were maneuvered apart, and formed into two different orbits on 17 April 2014, with two satellites (Swarm A and C) flying side-by-side at about 460 km, with east–west separation of 1.4 °, while the third satellite (Swarm B) was flying 50 km higher. Due to the precession of their orbits, Swarm A and C need about 133 days to fully cover the 24-hour local time at all locations, while Swarm B needs about 141 days (e.g., Xiong C et al., 2018).

One important objective of the Swarm mission is to monitor the Earth's upper atmosphere. Each of the Swarm spacecraft is equipped with an electric field instruments (EFI) package, which includes two thermal ion imagers (TIIs) and two Langmuir probes (LPs). The two TIIs are embedded perpendicular to each other in a rectangle faceplate (FP) of the Swarm ram panel; the two LPs are mounted quite close to the FP but separated by 30 cm on the earthward edge of the Swarm ram panel. The TIIs are used to measure the plasma drift velocity, while the LPs are used to derive the in situ electron density (N_e), ion density (N_i), electron temperature (T_e) and spacecraft potential (V_s). More details about the EFI and its working principles are provided by Knudsen et al. (2017).

2.2 Swarm Spacecraft Potential and Flags

For Swarm, the spacecraft potential is measured as the difference

between spacecraft electrical ground and the surrounding ambient plasma. In a classic sweep of LP (e.g., Mott-Smith and Langmuir, 1926), the applied bias voltage is incremented or decremented in small steps, yielding a "current voltage" or "I-V" characteristic; the plasma density, electron temperature, and satellite potential can be estimated from the "I-V" curves. However, the Swarm LP alternates between the classical sweep and a high frequency harmonic mode. The classic sweep mode is done only once every 128 s for a duration of 1 s; the high frequency mode operates the rest of the time. Knudsen et al. (2017) provide a detailed description of how to derive the plasma parameters and spacecraft potential from the high frequency harmonic mode of a Swarm LP (see their Section 3.3). Here, we don't repeat all the detailed steps, but instead provide just the final formula for deriving the spacecraft potential, in order to highlight the quantities that could affect the spacecraft potential derivation:

$$V_s = \frac{-(i_{lin} - i_{ret} + d_{ret}v_{ret} - d_{lin}v_{lin})}{d_{ret} - d_{lin}}, \quad (1)$$

where v_{lin} is the linear bias, v_{ret} the retarded bias (in energy units); i_{lin} is the linear current, i_{ret} the retarded current, and d_{lin} is the linear derivative, d_{ret} the retarded derivative (real parts of the admittances).

In this study, we used mainly the V_s and N_e measurements provided by the Swarm LP. One point we want to emphasize is the flags related to the Swarm spacecraft potential, which are provided in the Level-1B plasma data product. The detailed description of flags for V_s data is provided by Buchert et al. (2018); it is repeated in our Table 1. To exclude unreliable V_s values, we used only the V_s data when it is flagged as 20. The other point we want to note is that, in the latest updates of the Swarm Level-1B processor, the algorithm to estimate the N_e was changed to use the ion current; therefore, the latest plasma density product with baseline 05 from Swarm is N_i rather than N_e (Buchert et al., 2018). But due to the electric neutrality of the ionospheric plasma, we have assumed that the N_e and N_i are equal at Swarm altitudes.

Our statistical analysis focuses on data collected in Swarm's first five-years, from December 2013 to November 2018. A five-year period is sufficient to provide a relatively even distribution of Swarm orbits over season and local time (LT). As reported by Xiong C et al. (2022), during low solar flux years the N_i data derived from the Swarm LP were much larger than the N_e measured by the incoherent scatter radar (ISR) at Jicamarca. The cause of such a discrepancy between the two techniques is that in the Swarm LP processing algorithm the ions are assumed to be 100% O^+ at the Swarm altitude. However, due to the contraction of ionosphere to lower altitudes during low solar flux levels, light ions, e.g., H^+ or He^+, can diffuse down from the plasmasphere to the ionosphere, challenging the 100% O^+ assumption at the Swarm altitude and causing overestimation of N_i from the Swarm LP. Therefore, the N_i data used in this study have been normalized to reduce the solar flux influence, by use of Equations (3) and (4) of Xiong C et al. (2022).

3. Results

Figure 1 shows the distributions of V_s counts for each of the three Swarm satellites. For each satellite, the counts of V_s readings have been divided into bins with steps of 0.1 V. The V_s data from all three satellites show very similar distributions: almost all of the V_s readings fall within the range between −7.0 V and 0 V; very few V_s are out of this range. The Swarm V_s distribution confirms previous observations that the V_s of LEO satellites is almost always within a slightly negative potential range. There are two peaks of V_s, centered around −2 V and −5.5 V. Compared to the first peak, the count of readings at the second peak, centered around −5.5 V, is by about one order of magnitude lower. As Swarm A and C fly side by side, and the characteristics of their spacecraft potential are very similar, we will present only the results from Swarm A and Swarm B, to highlight the possible influence of altitude on spacecraft potential.

Based on the V_s distributions shown in Figure 1, the existence of two distinct V_s peaks suggest different sources; therefore, we have divided the V_s data into two categories: less-negative ($-5 < V_s < 0$ V) and more-negative ($-6.5 < V_s < -5$ V). We first examine their geographic distributions. For each category, the V_s values are first sorted into bins of latitude (2°) and longitude (5°). The mean values for each bin are then presented in Figure 2. In each panel, the magnetic latitude (Mlat) from −60° to 60° with steps of 30° are shown as thick black dashed lines. For Swarm A (top two panels of Figure 2), we see that both categories of V_s data exhibit clear dependence on magnetic latitude (Mlat), rather than geographic latitude.

Within the first, less-negative, V_s category ($-5 < V_s < 0$ V), the voltages are generally closer to zero at equatorial and low latitudes;

Table 1. Flags related to V_s listed in the Level-1B plasma data product of Swarm, which is intent to identify the possible error sources that could affect the V_s of Swarm.

Flags	Value	Description
Flags_ V_s	10 or 20	Nominal case
	25	ADC overflow at the retard bias, discarding V_s is recommended
	26	ADC overflow at the linear bias, discarding V_s is recommended
	30 or 35 or 45	Failed tracking (flag 30), possibly combined with retard overflows (flags 35 or 45), discarding V_s is recommended
	30 or 36 or 46	Failed tracking (flag 30), possibly combined with linear overflows (flags 36 or 46), discarding V_s is recommended
	33	Value of V_s is unreasonable, discarding V_s is recommended

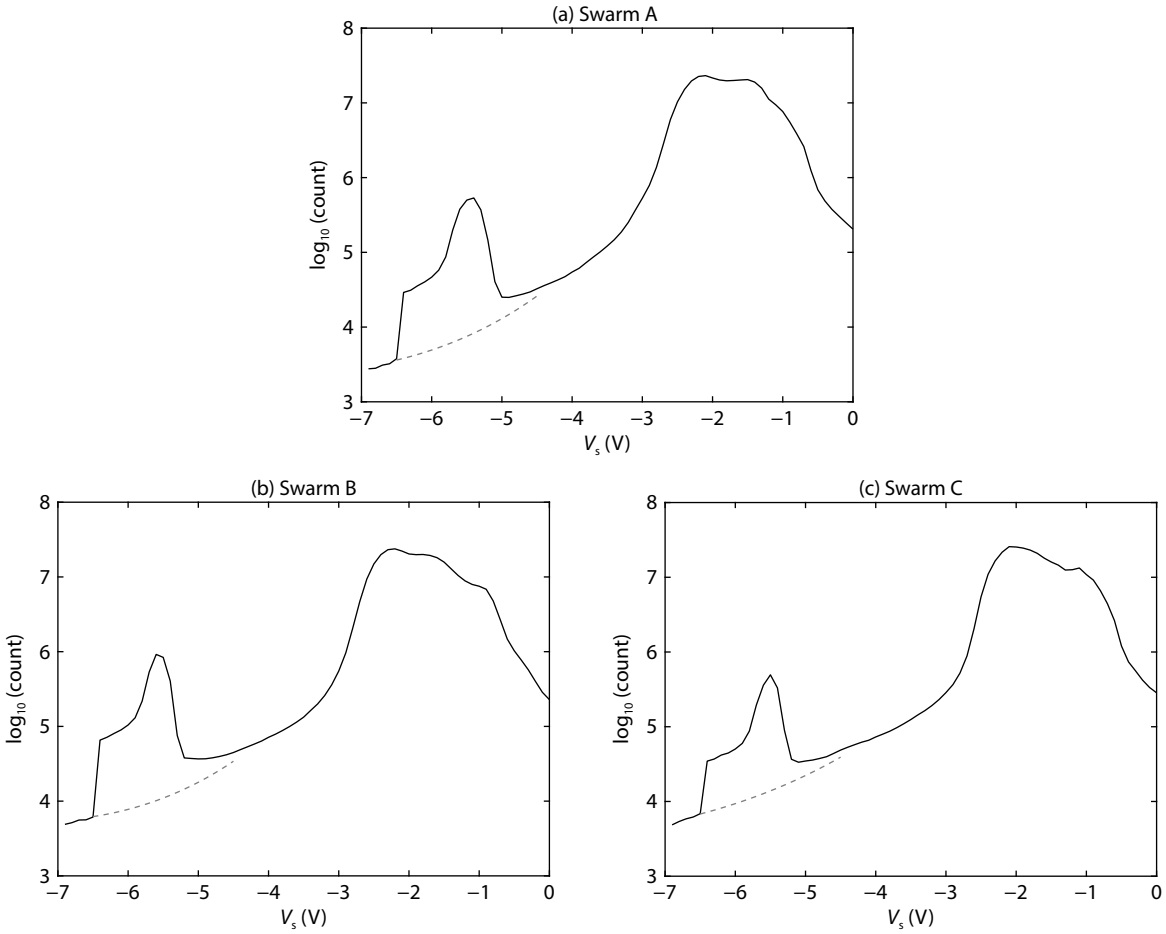

Figure 1. Logarithm distribution of counts for V_s of different values, separately for the three Swarm satellites.

indeed, the least-negative potential readings were recorded along the magnetic equator. In addition, in this range a notable longitudinal wave-4 structure of V_s is also evident at the equatorial and low latitudes. The ionospheric background density also shows a prominent longitude wave-4 pattern (e.g., Immel et al., 2006; Xiong C and Lühr, 2013), and this similarity suggests that this category of Swarm spacecraft potential readings is highly related to the background plasma density at Swarm altitudes. At high latitudes, these less-negative V_s readings are furthest from 0 V at locations close to the magnetic poles, e.g., around −90° E (close to the northern magnetic pole), and 130°E (close to the southern hemisphere's pole).

Within the second category (the more-negative V_s values, $V_s < -5$ V), the values closest to −5 V are found not along the magnetic equator, but appear, instead between 20°–50° Mlat in both hemispheres (the blank areas in these panels of Figure 2 are due to lack of valid observations). When looking at the longitudinal dependence of data in this deeper-negative category, we see that V_s values are relatively more negative (lower than −5 V) around the south Atlantic anomaly (SAA) regions, compared to the other longitudes of the middle latitudes.

The V_s readings observed by Swarm B (bottom two panels of Figure 2) are very similar to those from Swarm A. Comparing their less-negative readings, the average V_s data recorded at Swarm B are somehow lower by about 0.2 V than data in this same category collected in the same locations by Swarm A. Swarm B's second-category (more-negative) readings are again lower than Swarm A's, again by about 0.2 V, at latitudes further from the equator than ±60° Mlat; but V_s values recorded by both satellites between 20°–50° Mlat in both hemispheres were closely in agreement. Note here, again, that the blank (uncolored) areas within these Mlat regions in Figure 2 indicate a lack of valid observations. Different from Swarm A, the more-negative V_s values recorded by Swarm B at the SAA region extend from the southern hemisphere to the northern hemisphere.

Figure 3 presents the event numbers recorded by Swarm A and Swarm B in each geographic bin of latitude versus longitude, separately for the two V_s categories. We see that V_s events in the first category (Figures 3a and 3c) are almost evenly distributed at all latitudes and longitudes, with a mean event number of about 4×10^4; event numbers larger than this are seen only near the highest latitude of the Swarm orbits.

Highest V_s event counts in the second, more-negative, category (Figures 3b and 3d), were recorded at regions with |Mlat| > 50°; next-highest counts were observed in the magnetic equatorial region. The fewest events appeared in both hemispheres between 20°–50° Mlat. Thus, looking back at the V_s data in Figures 2b and 2d, we see that the relatively larger and sparsely

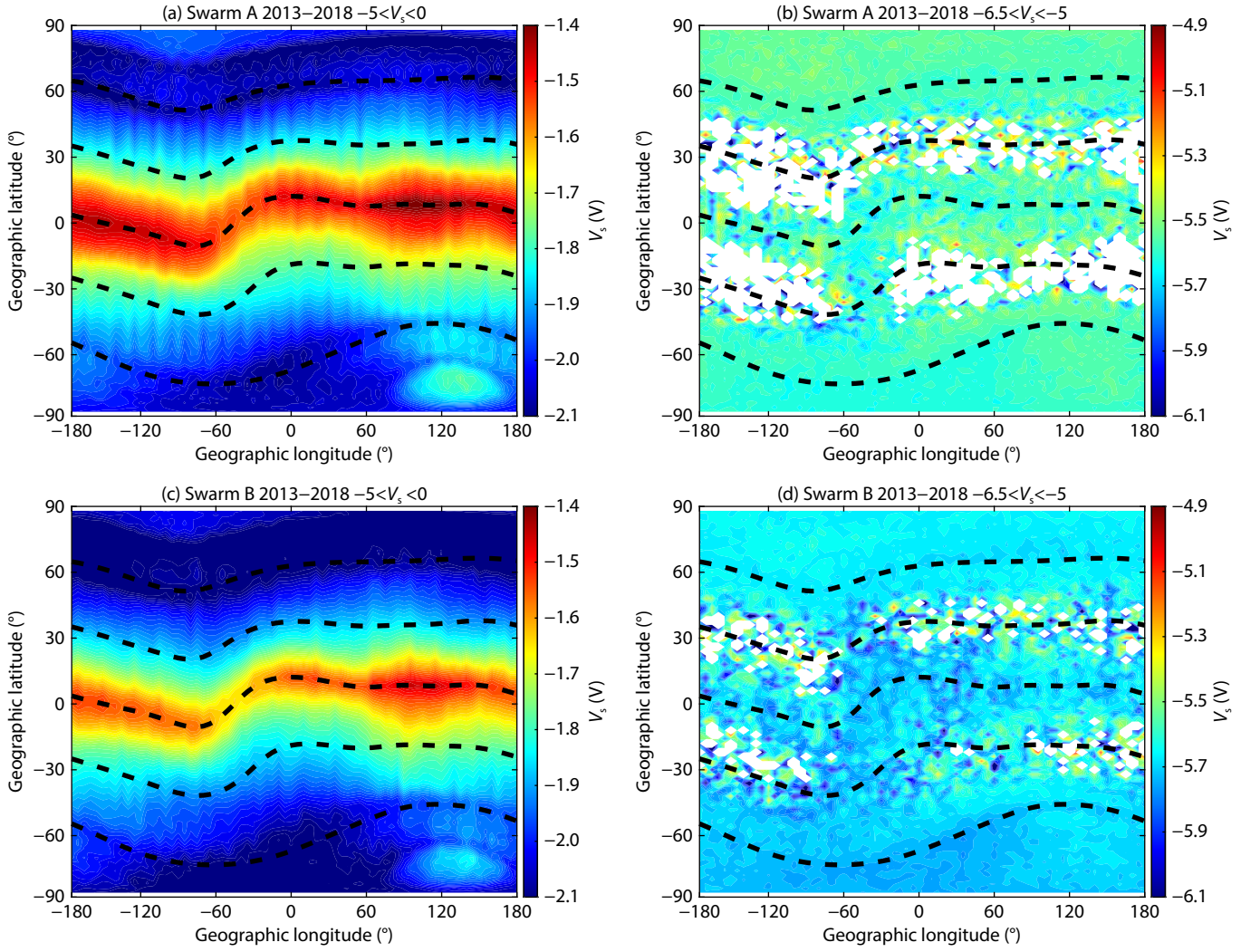

Figure 2. The geographic distribution of the mean V_s values for the two V_s categories: (left) $-5 < V_s < 0$ V and (right) $-6.5 < V_s < -5$ V. The top panels are the result from Swarm A, while the bottom panels are the results from Swarm B. In each panel, the Mlat from −60° to 60° with steps of 30° are shown as thick black dashed lines.

distributed V_s values in the two middle latitude bands in fact correspond to very few observations. In addition, compared to the northern high latitudes, many more events were observed in the corresponding latitudes in the southern hemisphere. For the longitudinal distribution at equatorial and low latitudes, two patches of events are found at the SAA (from −90°E to 0°) and Asian longitudes (30°–150°E), which is more prominent at the altitude of Swarm B.

In the next step, we checked the Mlat versus magnetic local time (MLT) distributions of V_s. Again, the V_s data have first been divided into the two categories: $-5 < V_s < 0$ V and $-6.5 < V_s < -5$ V. For each category, the V_s data have been sorted into 2° Mlat and 0.5 hour MLT bins. Figures 4 and 5, respectively, present each bin's mean V_s value and event number (the blank areas in Figures 4b, 4d and 5b, 5d indicate that no V_s events more negative than −5 V were observed within the corresponding bins).

A prominent feature seen in the first category of V_s data, Figures 4a and 4d, is that the relatively higher values (those closer to 0 V) were recorded on the nightside, compared to the dayside. The most negative V_s readings in this category were recorded near dawn at almost all latitudes; in the range |Mlat| = 30°–60°, such more-negative V_s readings continued to be observed until dusk, forming two prominent bands of dayside V_s readings in both hemispheres. When looking at the latitude dependence of V_s distribution in daytime, we observe that it is symmetrical about the magnetic equator, the V_s values tending to be least-negative close to the magnetic equator and growing more-negative as the satellites flew further from the magnetic equator.

However, the second category of V_s readings, those more negative than −5 V, is unevenly distributed over MLT (Figures 4b and 4d). Four V_s peaks can be seen at around 04:00, 09:00, 14:00 and 20:00 MLT, covering the Mlat bins from −50° to 50°. One interesting point is that these four peaks of MLT are very consistent from Swarm A and Swarm B, though the orbits of two satellites have different MLT processing rates. Comparing the V_s distributions between the two satellites, we see for both categories that the V_s values recorded by Swarm B are in general lower than Swarm A's by about 0.2 V.

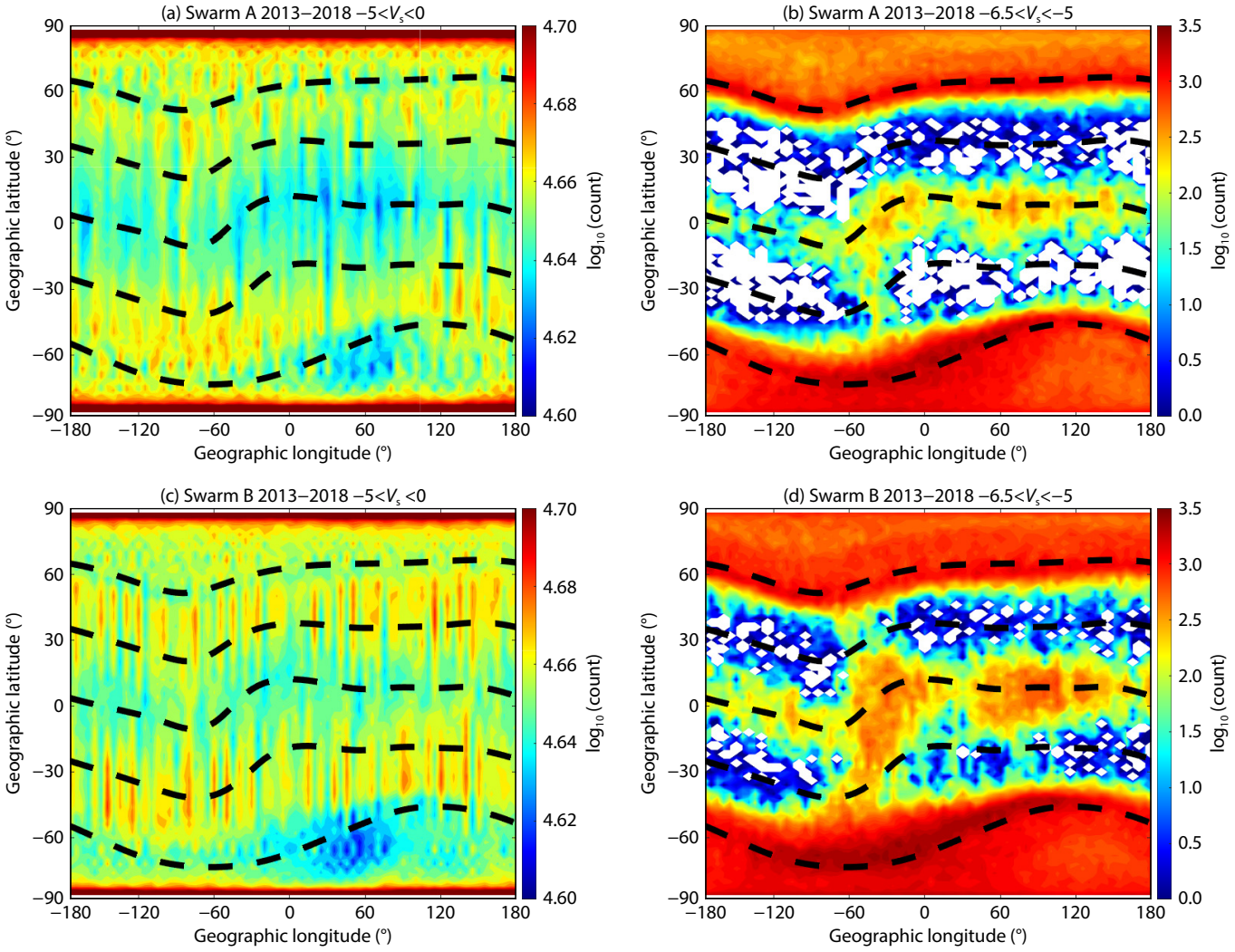

Figure 3. Colors reflect the V_s event number in each geographic latitude and longitude bin. Similarly, data have been sorted according to the two V_s categories, and separately for Swarm A and Swarm B.

Examination of the distributions of event numbers by Mlat versus MLT (Figure 5) reveals, as expected, that many more events were recorded in the first, less-negative, V_s category than in the second, more-negative, category. Interestingly, however, the event numbers in the first category are slightly smaller around the four MLT times, 04:00, 09:00, 14:00 and 20:00, at which V_s peaks appeared in the second category. In addition, many more first-category events were observed around −70° and 80° Mlat, forming two bands in the southern and northern high latitudes.

The highest event number counts in the second, more-negative, V_s category, were recorded at |Mlat| > 50° (Figures 5b and 5d). In general, more second-category events were recorded in the southern hemisphere than in the northern hemisphere; for both hemispheres, more events occurred on the nightside than on the dayside. Compared to the high latitudes, many fewer events were recorded at the low and middle latitudes. One exception is a detached island of observations recorded at the equator and low latitudes around dawn. The other observations clustered around 04:00, 09:00, 14:00 and 20:00 MLT, corresponding well to the four V_s peaks seen in Figures 4b and 4d, indicating that the relatively larger and sparsely distributed V_s values recorded in the four MLT sectors represent very few observations.

Figure 6 shows the Mlat versus seasonal variations of V_s values recorded by Swarm satellites A and B, separately for the two V_s categories. Here, the day of year (DoY) is used to represent the seasons. First-category V_s values (Figures 6a and 6c) exhibit dramatically different seasonal variations at low latitudes (|Mlat| < 30°) compared to middle and high latitudes. At low latitudes, the recorded V_s values tended to be at their least-negative around the two equinoxes but more negative around the June solstice. At middle and high latitudes in both hemispheres, however, seasonal variations were much more prominent; V_s values recorded in local winter were significantly more negative than in local summer.

Second-category V_s events, as previously mentioned, were rarely observed at low and middle latitudes, accounting for the many colorless regions in Figures 6b and 6d, which thus exhibit no clear seasonal variation. At high latitudes, however, in both hemispheres, the second-category V_s values recorded around local summer were somewhat less negative than those recorded

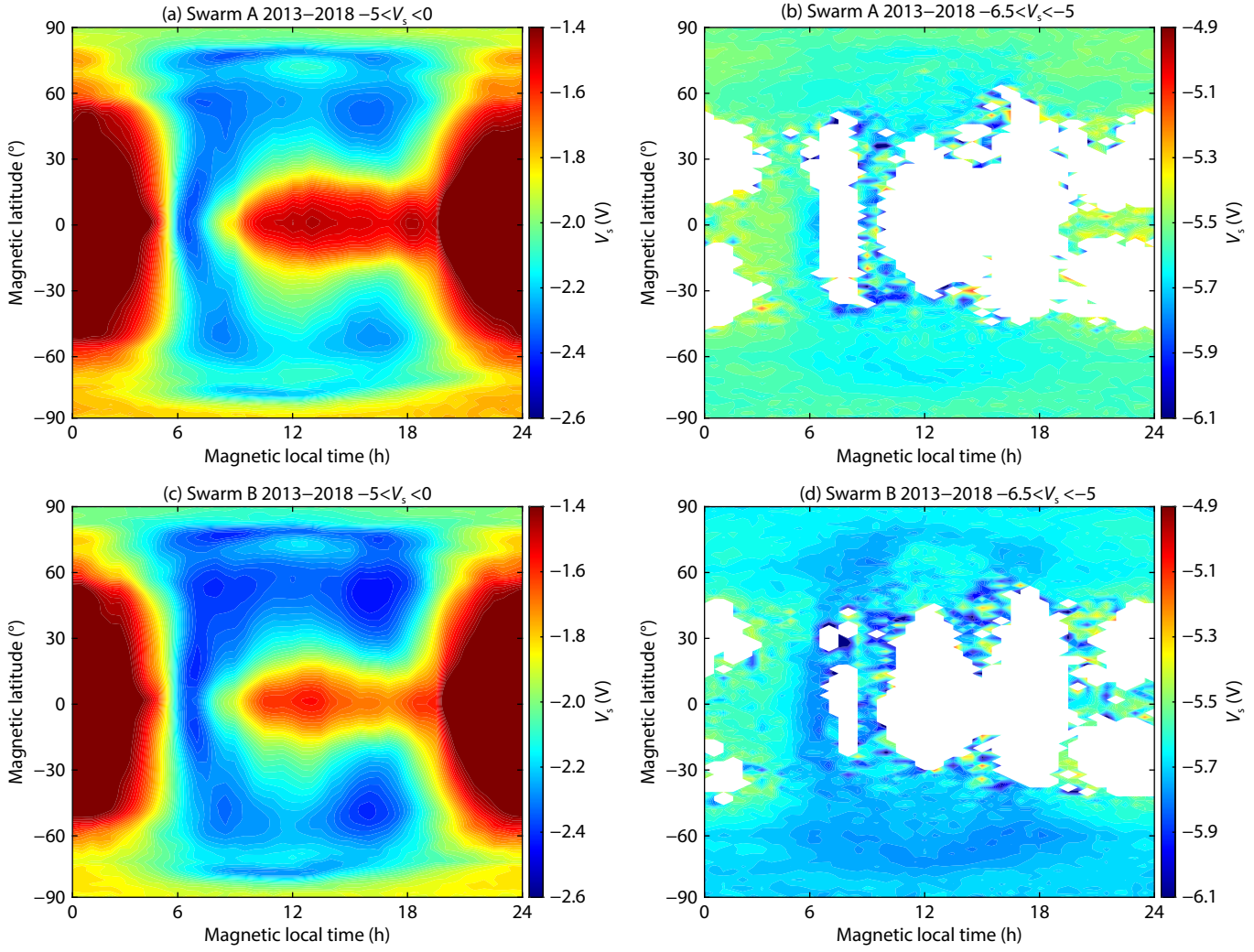

Figure 4. Colors indicate mean value of V_s recorded in each Mlat and MLT bin, for each of the two (less-negative versus more-negative) V_s categories.

around local winter; this is opposite to the pattern observed for first-category V_s seasonal observations at high latitudes.

Figure 7 presents the data coverage for the V_s distributions shown in Figure 6. Event numbers for first-category V_s observations exceed 1×10^4 in almost all bins (Figures 7a and 7c), more than sufficient to allow valid statistical analysis. For second-category V_s observations, most of the events counted were at high latitudes during local winter; the slightly more negative V_s values recorded in this second category at high latitudes around local summer correspond to very few observations.

4. Discussion

As mentioned in our introduction, spacecraft are generally slightly negatively charged because their ambient electron flux is relatively larger than the ion flux. This has been confirmed by the spacecraft potentials recorded by three Swarm satellites, as shown in Figure 1, with the majority of their readings averaging around −2.0 V. Though the spacecraft potential can vary between 0 V and −7 V, V_s readings typically exhibit global, seasonal, and MLT dependencies. And such dependencies are consistent between the observations from Swarm A/C and Swarm B satellites that fly at different altitudes, though the average V_s values recorded by Swarm B are by about 0.2 V more negative than those recorded by Swarm A. Our results suggest that the variations of spacecraft potential recorded by the Swarm satellites are due primarily to the instantaneous space environment at the satellites' altitudes.

4.1 Sources Contributing to the Spacecraft Potential

According to Garrett (1981), the basic equation expressing the current balance for a given surface in an equilibrium situation is:

$$I_E(V) - [I_I(V) + I_{SE}(V) + I_{SI}(V) + I_{BSE}(V) + I_{PH}(V) + I_B(V)] = I_T, \quad (2)$$

where V is the satellite potential caused by the different currents, I_E is the incident electron current on satellite surface, I_I is the incident ion current on the satellite surface, I_{SE} is the secondary electron current due to I_E, I_{SI} is the secondary electron current due to I_I, I_{BSE} is the backscattered electron current due to I_E, I_{PH} is the photoelectron current, I_B is the current from active sources such as charged particle beams or ion thrusters, and I_T is the total current to the satellite (at equilibrium, $I_T = 0$).

Of these currents, the incident electrons and ions are determined by the background plasma and incident energetic particles in the

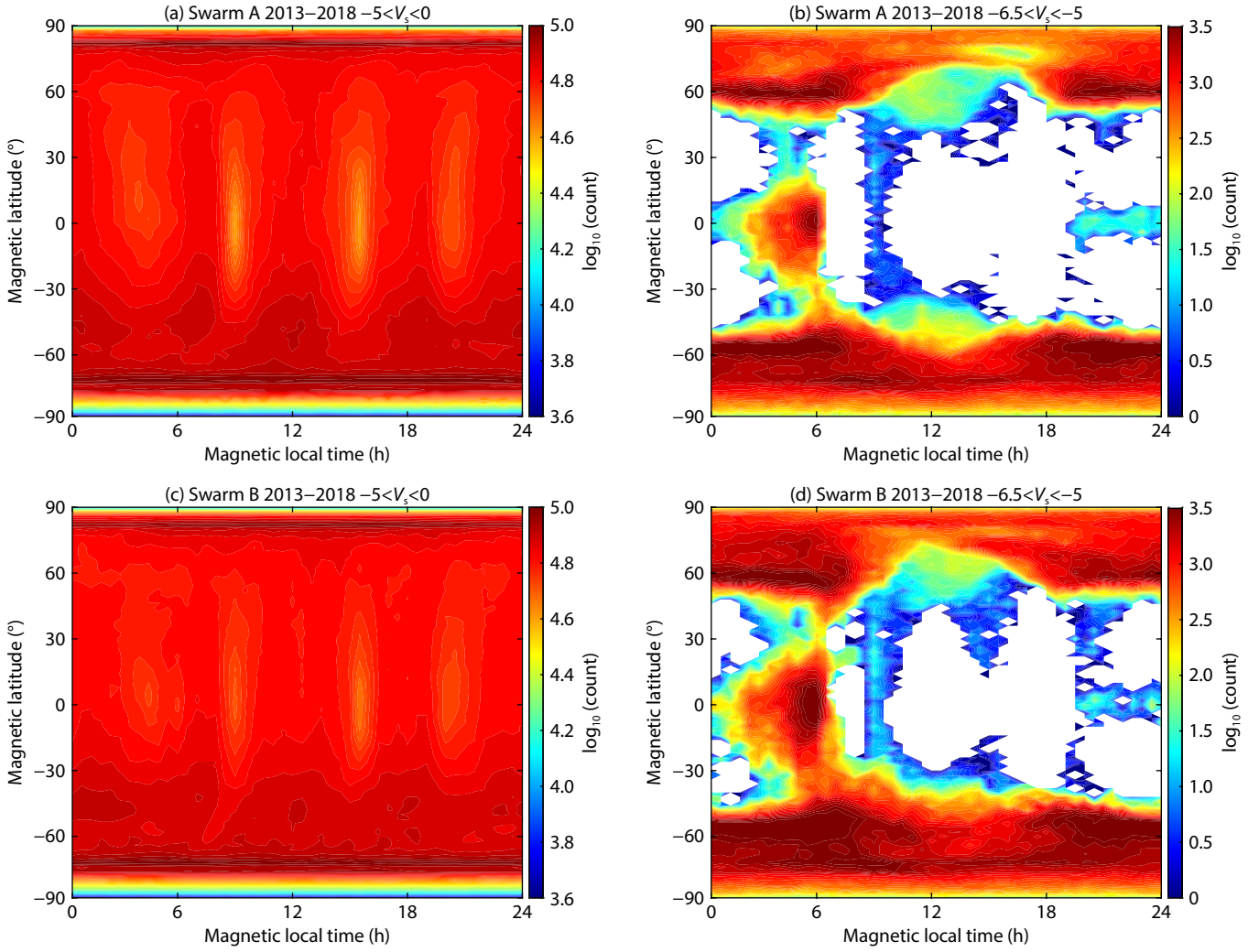

Figure 5. Colors indicate number of events recorded in each Mlat and MLT bin.

satellite's orbit; the photoelectron current is determined primarily by the sunshine; the secondary and backscatter electron currents depend not only on the incident particles and photoelectrons, but also on the materials of the spacecraft's panels. From Equation (1) we know that the spacecraft potential is mainly determined by the incident fluxes of electrons and ions on the satellite surface, but both the background plasma density and precipitating particles from the magnetosphere can influence those electron and ion fluxes. Therefore, below we discuss qualitatively the possible influences on spacecraft potential from precipitating particles and background plasma density.

4.2 Influence of Precipitating Particles

As reported by Anderson (2012), most of the very negative charge events of DMSP were observed when the satellites entered the auroral zone, where the energetic particles precipate much more easily into the lower atmospheric altitudes. Compared to the first less-negative category of V_s events, the second, more deeply-negative, category seems to be more likely caused by the precipitating electrons. Supporting evidence includes, e.g., prominently lower V_s values found at the SAA region, where the background magnetic field intensity is much lower than at the other longitudes, allowing energetic particles to precipitate much more easily to the Swarm altitudes. Additional support is that V_s values recorded in the geographical polar regions are relatively higher (less negative) nearest to the magnetic poles. Such a feature can be understood as follows: all the magnetic field lines converge at the magnetic pole, so the field intensity is much stronger there than anywhere else. The stronger magnetic field makes it relatively difficult for the energetic particles to precipitate to the Swarm altitudes, compared to other longitudes at high latitude regions. The third supporting observation is that V_s values observed at high latitudes during local summer (see Figures 6b and 6c) were relatively less negative. According to Anderson (2012), most of the spacecraft charging events of DMSP caused by precipitated electrons were observed in the auroral oval, during a low solar activity year when the background plasma density was low. At high latitudes, the neutral thermosphere in the summer hemisphere is denser than in the winter hemisphere; therefore, the precipitated electrons are much more easily absorbed by the neutrals. In addition, the sunlight-caused ionization is much larger during local summer than during local winter; therefore the background plasma density is also relatively larger in the summer hemisphere. Assuming that the precipitating energetic electrons have the

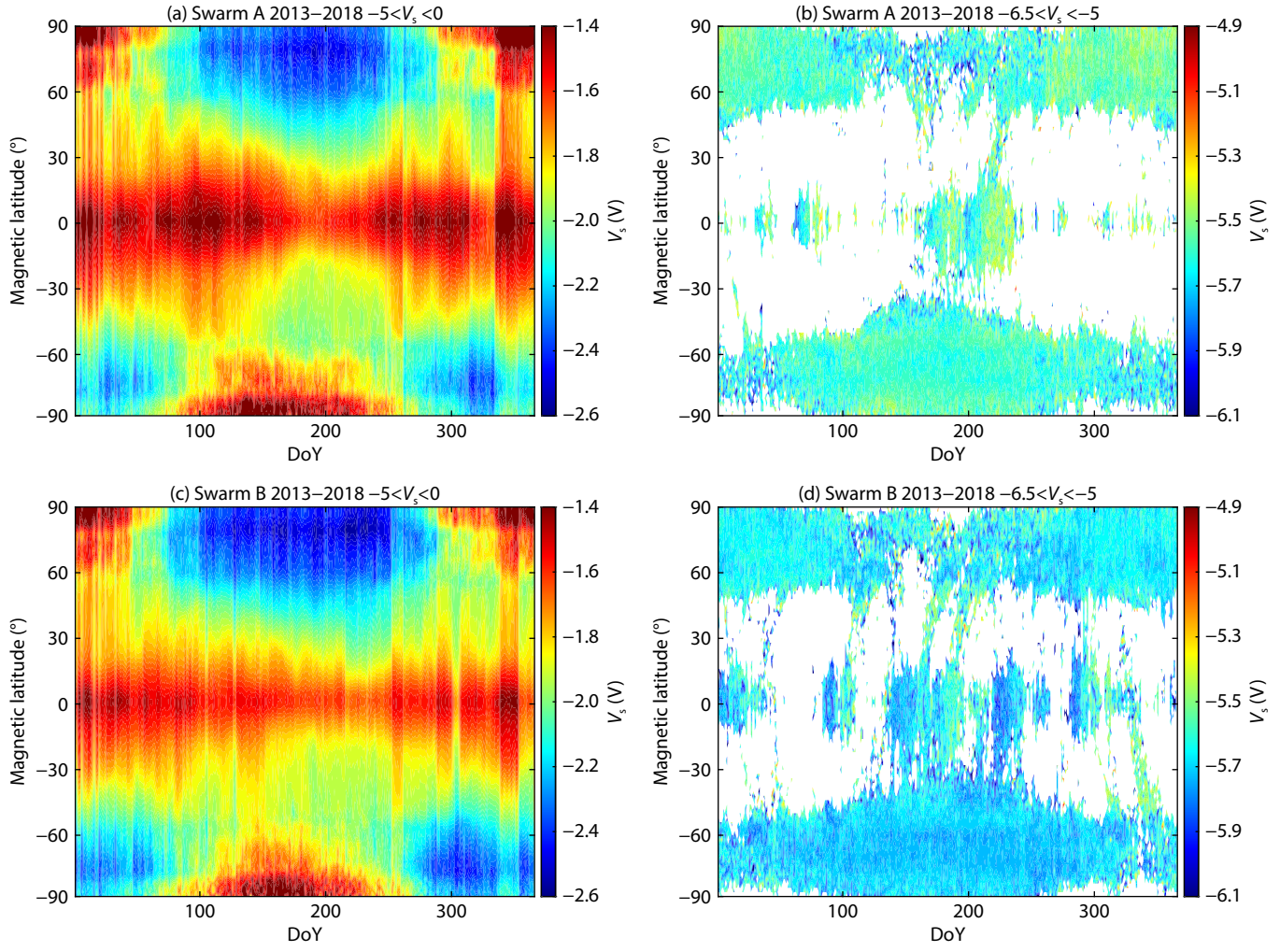

Figure 6. Colors indicate mean value of V_s for each Mlat and DoY bin.

same number flux in the two hemispheres, they will be more easily trapped by the ions, and will thus constitute a relatively lower portion of the charge, in the hemisphere with the greater plasma density, namely the summer hemisphere. The two reasons above may explain why, for the second category of V_s data, the Swarm observations were relatively less-negative in high latitudes during local summer.

However, it is a pity that no instrument on board the Swarm satellites was measuring the flux of energetic particles. To better visualize their influence on spacecraft potentials at Swarm altitudes, we choose the most intense geomagnetic storm during the Swarm mission period, which was the well-known St. Patrick's Day storm that happened on 17–18 March 2015. The top panel of Figure 8 shows the variations of the *Dst* index from 16 to 19 March, with its minimum value reaching about −234 nT at 2200 coordinated universal time (UTC) on 17 March. As seen from the middle and bottom panels, at high latitudes the V_s values recorded by both Swarm A and Swarm B became more negative starting on March 17, corresponding to the main phase of the geomagnetic storm. As known, the flux of high energy electrons can be significantly larger during geomagnetic storms, and thus we see the outer layers of the Swarm being charged to much more negative voltages. In addition, the lowered spacecraft potential extends from about ±60° Mlat to about ±45° Mlat, from storm onset to storm main phase. This result suggests that the auroral zone typically extends to lower Mlats during enhanced magnetic activity, which is also consistent with earlier model predictions about the location of auroral ovals (e.g., Holzworth and Meng, 1975; Xiong C and Lühr, 2014; Xiong C et al., 2014).

In addition, significant V_s differences are seen between Swarm's ascending and descending orbits, located around 19:30/07:30 LT and 21:00/09:00 LT for Swarm A and Swarm B, respectively. Negative charge is more prominent during the descending orbits around 07:30/09:00 LT than during the ascending orbits around 19:30/21:00 LT.

4.3 Influence of the Background Plasma Density

With regard to the possible influence of background plasma density on the spacecraft potentials recorded by Swarm satellites, we suggest that the second, more-negative, category of Swarm V_s observations is more closely related to precipitating energetic electrons from the magnetosphere, whereas the first category, the V_s readings between −5 and 0 V, are more likely to be related to the distributions of background plasma.

As Figure 1 makes clear, 90% of total Swarm V_s observations fall

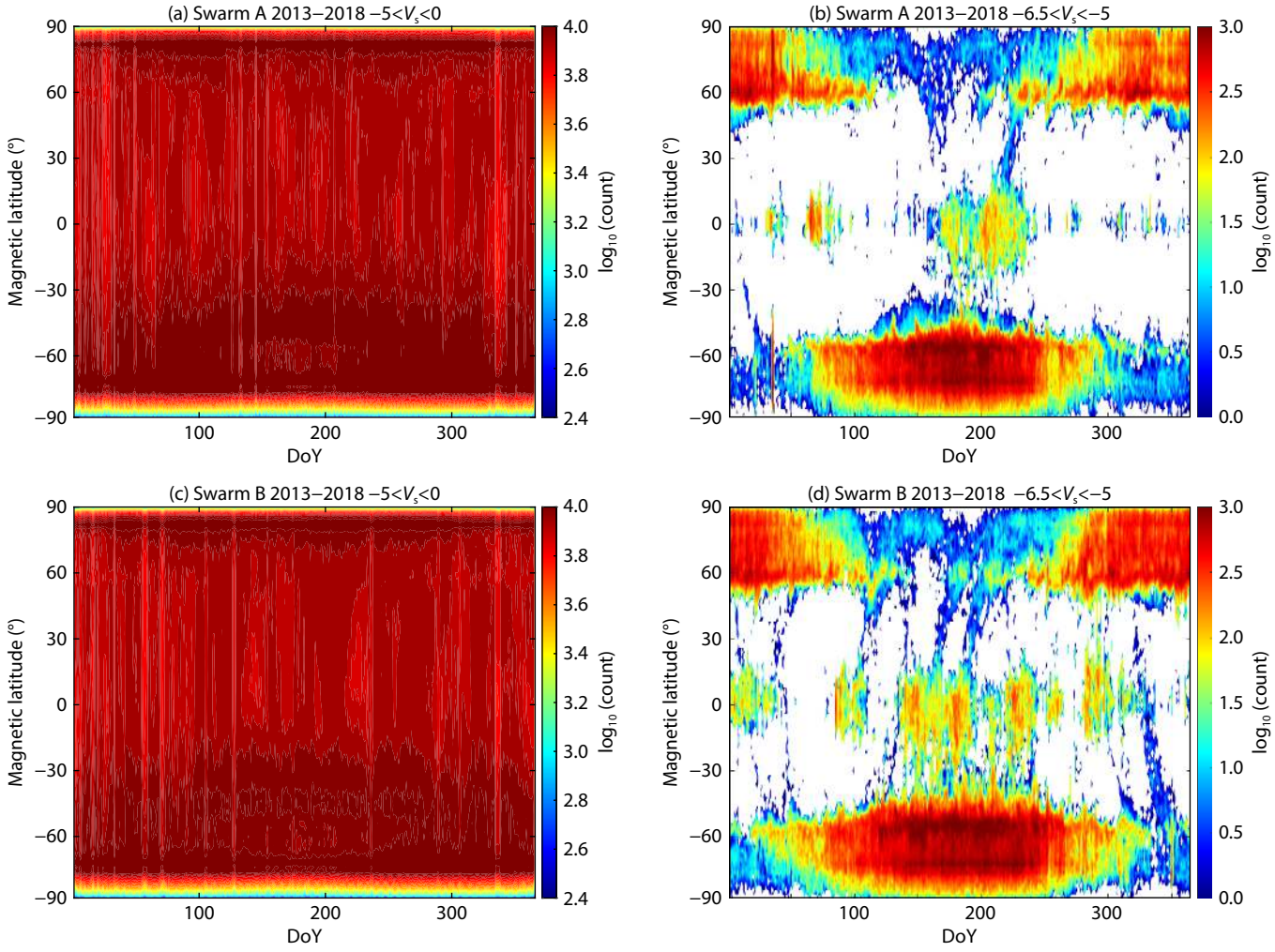

Figure 7. Colors indicate the event number in each Mlat and DoY bin.

into the first, less-negative, category, thus most of the V_s variations observed, most of the time, were in this range from −5 to 0 V. In this category, as shown in Figure 4, the spacecraft potential was much more negative on the dayside than on the nightside, which strongly suggests that the much denser background plasma explains Swarm's more negative V_s readings in this category. This conclusion is further supported by the seasonal variations of the V_s data, as shown in Figure 6: much more negative V_s values were recorded during local summer in the high latitudes, where the background plasma density is higher.

To better quantify this relationship, the event count of N_e data have again been divided into the two V_s categories, $-5 < V_s < 0$ V or $-6.5 < V_s < -5$ V, and then sorted into bins, separately for Swarm A (Figure 9) and Swarm B (Figure 10). At first look, the N_e distributions, including geographic latitude versus longitude (top panels), Mlat versus MLT (middle panels), as well as Mlat versus DoY (bottom panels), from Swarm A and Swarm B are very consistent between both V_s categories. As expected, at high latitudes the N_e counts are larger during local summer (left bottom panels of Figures 9 and 10), corresponding well to the much more negative V_s values shown at high latitudes in the left panels of Figure 6. In addition, at low and middle latitudes, larger N_e counts are observed on the dayside (left middle panels of Figures 9 and 10), corresponding well to the much more negative dayside V_s values at those latitudes. For the Mlat distributions, N_e counts are lower above the magnetic equator compared to counts at the crests of the equatorial ionization anomaly (EIA) (left top panels of Figures 9 and 10); again, V_s values reflect the difference in counts: potentials are less negative above the magnetic equator compared to values at the EIA crest (left panels of Figure 2).

So, for the first V_s category, V_s values are more negative at regions with higher background N_e, which is opposite to the pattern seen in data for the second, more deeply negative, V_s category.

As previously mentioned, the typical slightly negatively-charged spacecraft potentials recorded by Swarm are caused by the flux differences between ambient electrons and ions incident on the Swarm satellites. For the background cold plasma, the electron density is assumed to be equal to the ion density; therefore, differences in electron flux are expected to be larger when the background plasma density is larger, and V_s should be more negative at regions with larger plasma density. However, exceptions are observed. For example, at equatorial and low latitudes the background plasma density is usually larger during equinoxes than during the June solstice (see left bottom panels of Figures 9 and 10), but the observed V_s values (left panels of Figure 6) at these

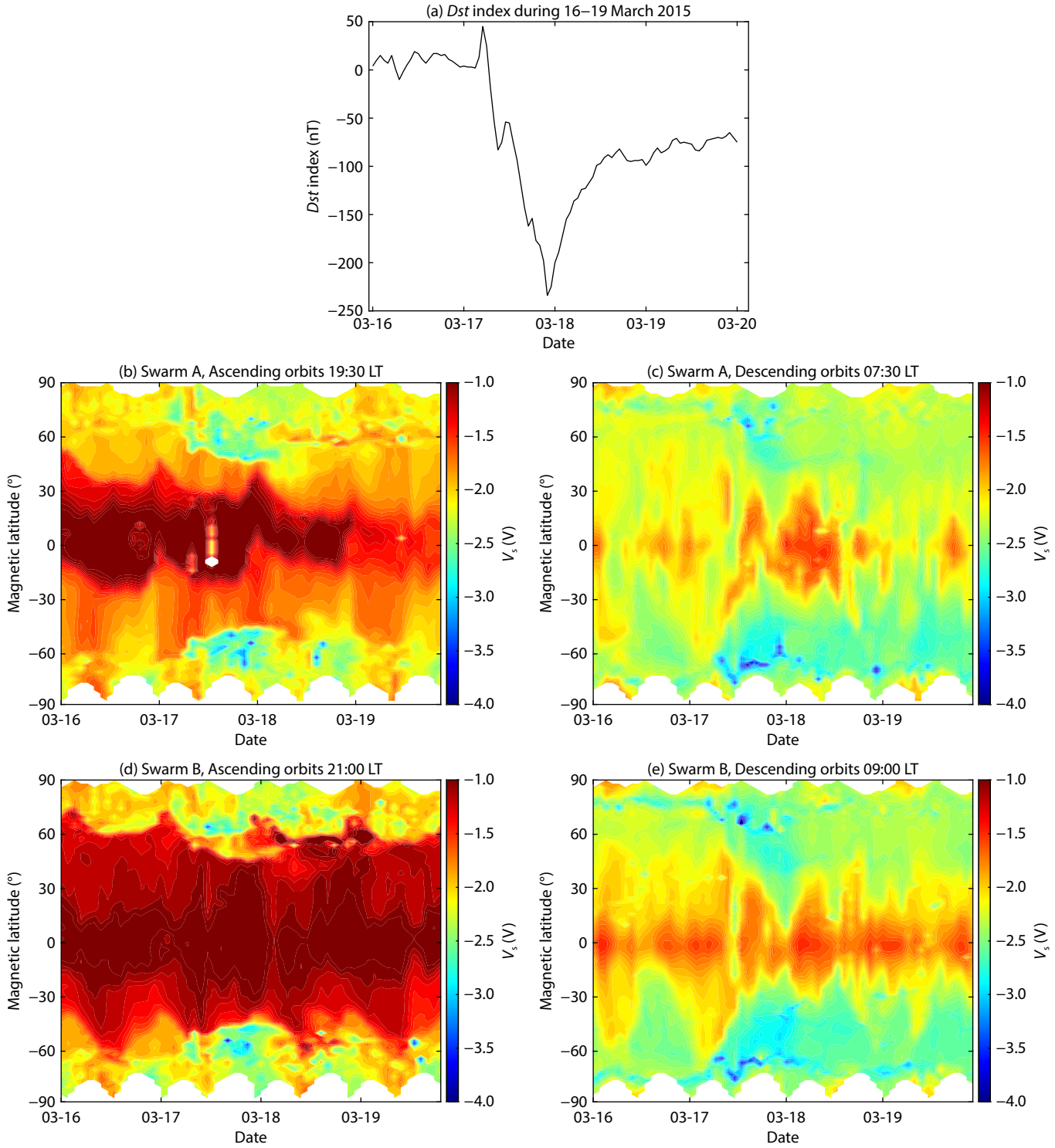

Figure 8. (a) The variation of *Dst* index during 16–19 March 2015. The Mlat versus time variations of V_s of Swarm A during its ascending and descending orbits are presented in panels (b) and (c); the results from Swarm B are presented in panels (d) and (e).

latitudes are somehow less negative during equinoxes than during the June solstice.

Though we do not at this time have an explanation for the different relationship between V_s and background plasma density at different latitudes, the derived V_s distributions are rather consistent between Swarm A and B. From the above analysis it seems that the influence of background "cold" plasma on the spacecraft potential of LEO satellites is more complicated than just the influence of precipitated "hot" plasma. Comparing the absolute values of the background plasma density, we see that the N_e values associated with the second V_s category (right panels of Figures 9 and 10) are lower by almost one order of magnitude than those associated with the first category (left panels of Figures 9 and 10). Though in this study we have divided the V_s of Swarm into two

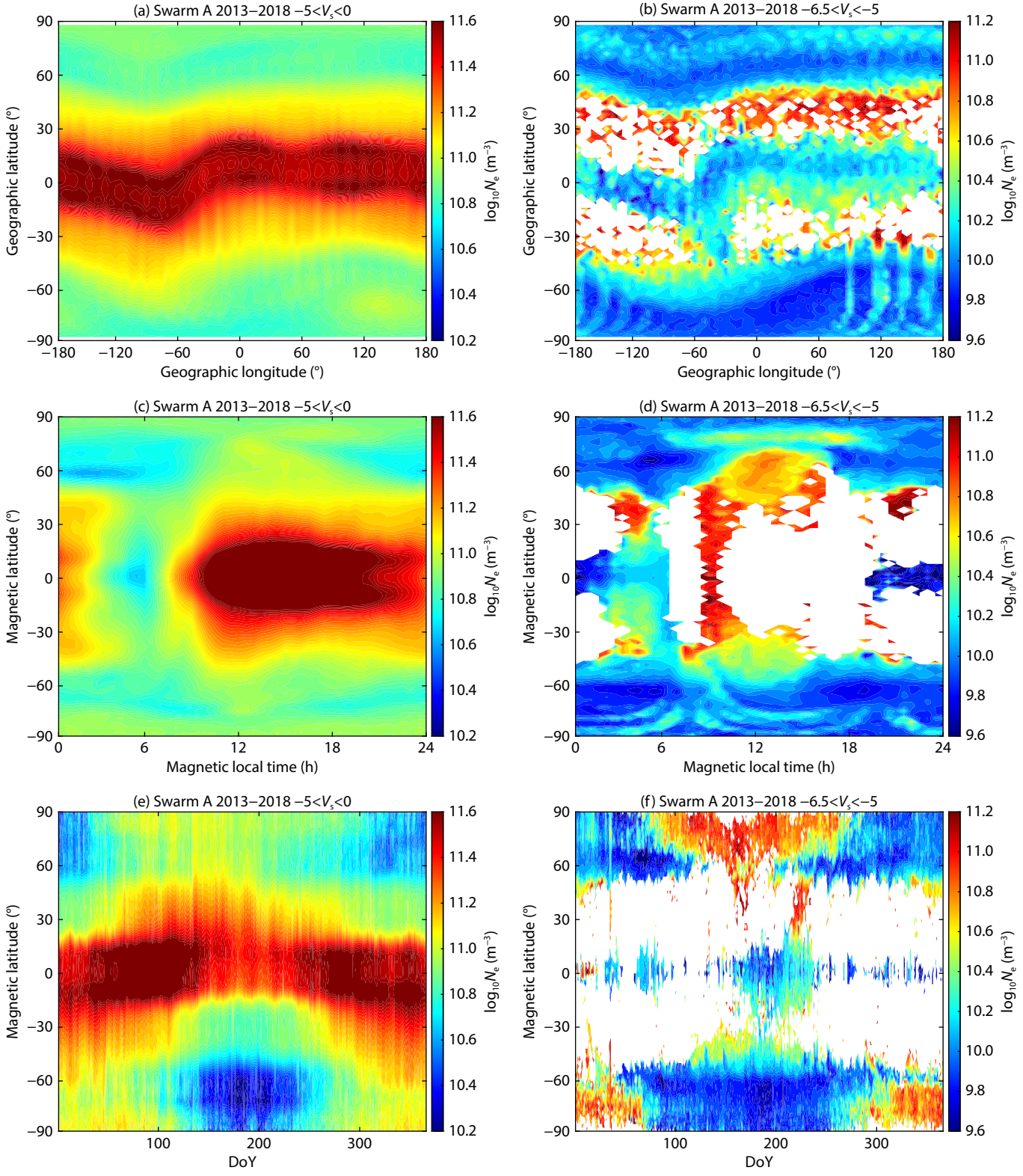

Figure 9. Colors indicate the mean value of background plasma density measured by Swarm A, separately for the two V_s categories: (left) $-5 < V_s < 0$ V and (right) $-6.5 < V_s < -5$ V. Plasma density is sorted into: (top) geographic latitude versus longitude; (middle) Mlat versus MLT; (bottom) Mlat versus DoY.

categories, we cannot totally separate the two categories in our analysis. As indicated in Figure 1, the events covered by the dashed line between −6.5 and −5 V in fact are the extension of the first category events. To have better visualization of the second category events, Figure 11 shows the event number distribution in the frame of N_e versus V_s. We see that in fact only the events within the "red eye" of higher event number and lower N_e values should be classified to the second category related to particle

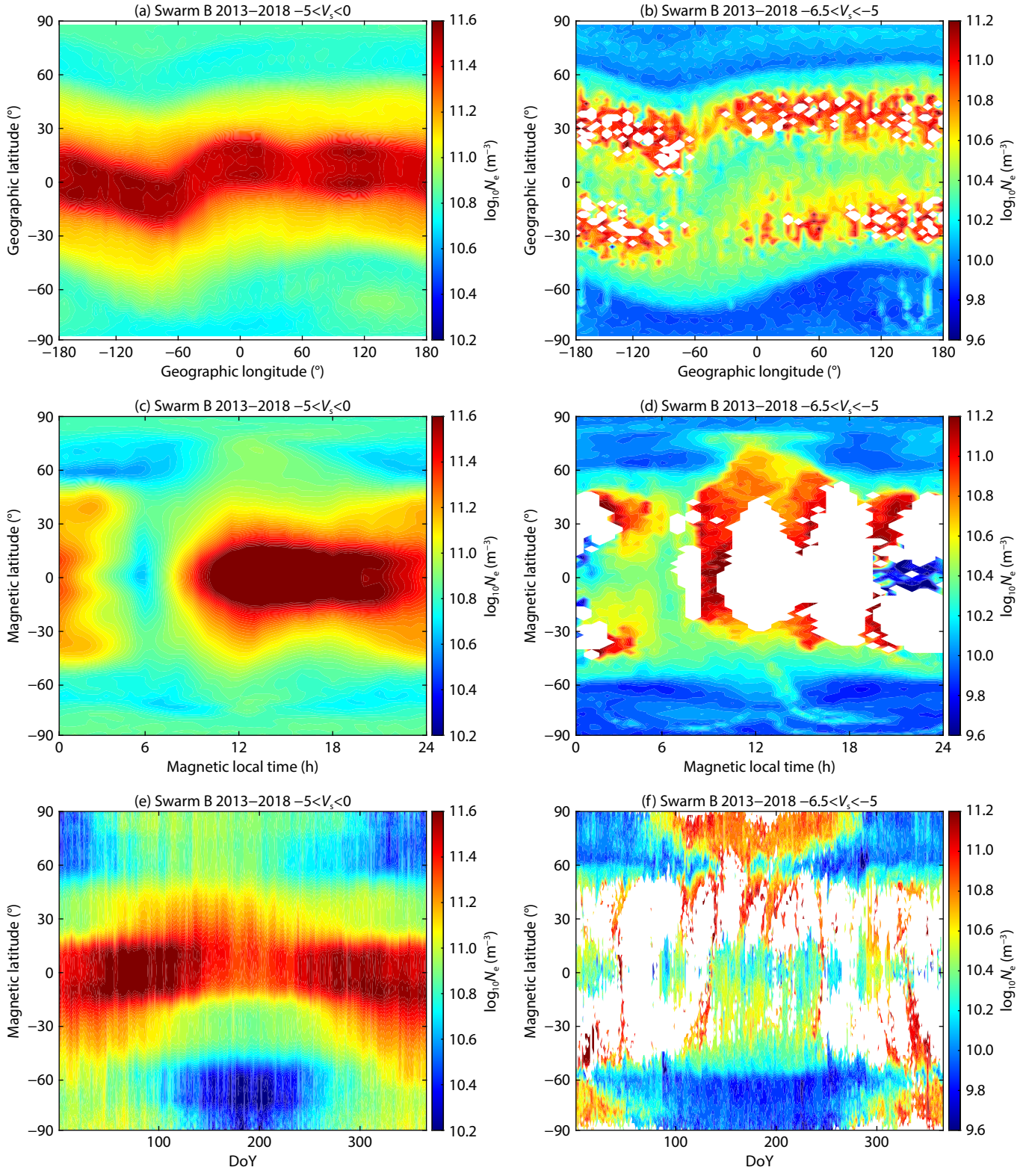

Figure 10. Similar to Figure 9, but for the mean values of background plasma density measured by Swarm B.

precipitations. The relatively sparsely distributed events in the currently used second category, e.g., those between ±20°–±50° Mlat (in Figures 2 and 3), those around 04:00, 09:00, 14:00 and 20:00 MLT (in Figures 4 and 5), as well as those in the high latitudes during local summer hemisphere (in Figures 6 and 7), correspond to the parts covered by the dashed lines in Figure 1, which should be classified in the first category.

In conclusion, our result suggests that when the background plasma is high, the V_s of a LEO satellite is mainly determined by the cold plasma; when the background plasma is low, the V_s of a LEO satellite is mainly determined by the energetic particles

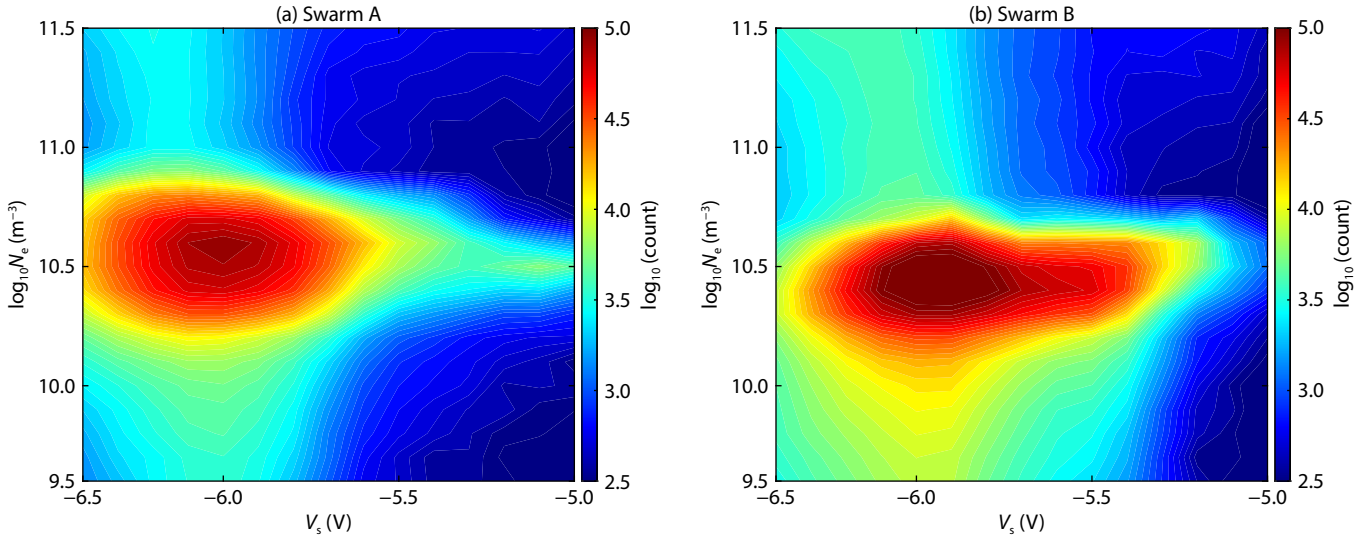

Figure 11. The event number distributions in the frame of N_e versus V_s, separately for Swarm A and Swarm B. Here, we considered only the second (more negative) V_s category, $-6.5 < V_s < -5$ V.

precipitating to the satellite altitude.

5. Summary

In this study, we have provided a detailed analysis of spacecraft potential (V_s) variations recorded by the Swarm satellites at about 400–500 km. To our knowledge, this is the first paper to focus on the Swarm spacecraft potential measurements, which differ significantly from the extreme charging events (usually with spacecraft potential as negative as −100 V) that have been the focus of previous studies. The variation of Swarm V_s readings falls within a few negative volts. To make our analysis and results reliable, we have carefully selected the data, using only V_s observations that are flagged as good quality. Our main findings are summarized as:

(1) As proved by the Swarm observations, spacecraft at LEO altitudes are charged just slightly negatively. For Swarm, the potential varies between −7 V and 0 V, with the majority of observations falling around −2 V. Interestingly, a second peak of V_s readings is found at −5.5 V, though the event numbers for these more-negative readings are lower by an order of magnitude than the approximately −2 V readings. We suggest that these two categories of V_s potentials are likely to have different causes.

(2) Accordingly, we divided the spacecraft potential data into two categories for further analysis: less-negatively charged ($-5 < V_s < 0$ V) and more-negatively-charged ($-6.5 < V_s < -5$ V). The two categories differ in their spatial and temporal distributions. The first, less-negative, category of V_s readings were closer to 0 V above the magnetic equator, but were much more negative on the night side; at high latitudes, they were relatively negative during local summer. The second, more-negative, category cluster into two bands at the middle latitudes (between ±20°–50° Mlat), with values close to the −5 V category threshold but with slightly lower values recorded at the SAA region; at high latitudes, the V_s values were relatively more negative during local winter — a pattern opposite to the one described, above, for the first (less-negative) V_s category.

(3) By comparing V_s readings to the distributions of background plasma density at Swarm altitudes, we find that, in the first category, the more negative potentials were recorded at regions with higher background plasma density. In the second category, however, the relationship is reversed: the more negative V_s readings were recorded at regions with lower background plasma density. This difference can be explained as follows: the difference between electron and ion fluxes incident on Swarm surfaces, which determines the spacecraft potential, is dominated by the background cold plasma in the first V_s category ($-5 < V_s < 0$ V), but by the precipitated energetic particles (hot plasma) in the second category ($-6.5 < V_s < -5$ V).

Acknowledgments

The authors want to thank Prof. Dr. Hermann Lühr for his fruitful discussion. This work is supported by the National Key R&D Program of China (Grant No. 2022YFF0503700), and the special found of Hubei Luojia Laboratory (220100011). Chao Xiong is supported by the Dragon 5 cooperation 2020–2024 (project no. 59236). The Swarm data are provided by ESA at https://earth.esa.int/web/guest/swarm/data-access, and the *Dst* index is available at OMNIWeb database https://omniweb.gsfc.nasa.gov/.

References

Allen, J. (2010). The Galaxy 15 anomaly: another satellite in the wrong place at a critical time. *Space Wea.*, *8*(6), S06008. https://doi.org/10.1029/2010SW000588

Anderson, P. C. (2012). Characteristics of spacecraft charging in low Earth orbit. *J. Geophys. Res.: Space Phys.*, *117*(A7), A07308. https://doi.org/10.1029/2011JA016875

Buchert, S. (2018). Langmuir probe level 1b algorithm. Retrieved from https://earth.esa.int/eogateway/documents/20142/37627/swarm-level-1b-plasma-processor-algorithm.pdf/bae64759-b901-d961-4d18-0a5b317f8c12

DeForest, S. E. (1972). Spacecraft charging at synchronous orbit. *J. Geophys. Res.*, *77*(4), 651–659. https://doi.org/10.1029/ja077i004p00651

Frooninckx, T. B., and Sojka, J. J. (1992). Solar cycle dependence of spacecraft charging in low Earth orbit. *J. Geophys. Res.: Space Phys.*, *97*(A3), 2985–2996. https://doi.org/10.1029/91ja02704

Garrett, H. B. (1981). The charging of spacecraft surfaces. *Rev. Geophys.*, *19*(4), 577–616. https://doi.org/10.1029/RG019i004p00577

Holzworth, R. H., and Meng, C. I. (1975). Mathematical representation of the auroral oval. *Geophys. Res. Lett.*, *2*(9), 377–380. https://doi.org/10.1029/GL002i009p00377

Immel, T. J., Sagawa, E., England, S. L., Henderson, S. B., Hagan, M. E., Mende, S. B., Frey, H. U., Swenson, C. M., and Paxton, L. J. (2006). Control of equatorial ionospheric morphology by atmospheric tides. *Geophys. Res. Lett.*, *33*(15), L15108. https://doi.org/10.1029/2006GL026161

Knudsen, D. J., Burchill, J. K., Buchert, S. C., Eriksson, A. I., Gill, R., Wahlund, J. E., Åhlen, L., Smith, M., and Moffat, B. (2017). Thermal ion imagers and Langmuir probes in the Swarm electric field instruments. *J. Geophys. Res.: Space Phys.*, *122*(2), 2655–2673. https://doi.org/10.1002/2016JA022571

Lai, S. T., and Cahoy, K. (2016). Spacecraft charging. In J. L. Shohet (Ed.), *Encyclopedia of Plasma Technology* (pp. 1352–1366). Boca Raton: CRC Press. https://doi.org/10.1081/e-eplt-120053644

Matéo-Vélez, J. C., Sicard, A., Payan, D., Ganushkina, N., Meredith, N. P., and Sillanpää, I. (2018). Spacecraft surface charging induced by severe environments at geosynchronous orbit. *Space Weather*, *16*(1), 89–106. https://doi.org/10.1002/2017SW001689

Mott-Smith, H. M., and Langmuir, I. (1926). The theory of collectors in gaseous discharges. *Phys. Rev.*, *28*(4), 727–763. https://doi.org/10.1103/PhysRev.28.727

Wright, K. H., Swenson, C. M., Thompson, D. C., Barjatya, A., Koontz, S. L., Schneider, T. A., Vaughn, J. A., Minow, J. I., Craven, P. D., … Bui, T. H. (2008). Charging of the international space station as observed by the floating potential measurement unit: initial results. *IEEE Trans. Plasma Sci.*, *36*(5), 2280–2293. https://doi.org/10.1109/TPS.2008.2003257

Xiong, C., and Lühr, H. (2013). Nonmigrating tidal signatures in the magnitude and the inter-hemispheric asymmetry of the equatorial ionization anomaly. *Ann. Geophys.*, *31*(6), 1115–1130. https://doi.org/10.5194/angeo-31-1115-2013

Xiong, C., and Lühr, H. (2014). An empirical model of the auroral oval derived from CHAMP field-aligned current signatures—Part 2. *Ann. Geophys.*, *32*(6), 623–631. https://doi.org/10.5194/angeo-32-623-2014

Xiong, C., Lühr, H., Wang, H., and Johnsen, M. G. (2014). Determining the boundaries of the auroral oval from CHAMP field-aligned current signatures—Part 1. *Ann. Geophys.*, *32*(6), 609–622. https://doi.org/10.5194/angeo-32-609-2014

Xiong, C., Stolle, C., and Park, J. (2018). Climatology of GPS signal loss observed by Swarm satellites. *Ann. Geophys.*, *36*(2), 679–693. https://doi.org/10.5194/angeo-36-679-2018

Xiong, C., Jiang, H. C., Yan, R., Lühr, H., Stolle, C., Yin, F., Smirnov, A., Piersanti, M., Liu, Y. W., … Bilitza, D. (2022). Solar flux influence on the in-situ plasma density at topside ionosphere measured by Swarm satellites. *J. Geophys. Res.: Space Phys.*, *127*(5), e2022JA030275. https://doi.org/10.1029/2022ja030275

Ye, Y. G., Zou, H., Zong, Q.-G., Chen, H. F., Zou, J. Q., Shi, W. H., Yu, X. Q., Zhong, W. Y., Wang, Y. F., … Hao, X. Y. (2021). Energetic electron detection packages on board Chinese navigation satellites in MEO. *Earth Planet. Phys.*, *5*(2), 158–179. https://doi.org/10.26464/epp2021021